Electrochimica Acta 297 (2019) 676–684

Contents lists available at ScienceDirect

Electrochimica Acta

journal homepage: www.elsevier.com/locate/electacta

H_2S corrosion of mild steel: A quantitative analysis of the mechanism of the cathodic reaction

Aria Kahyarian*, Srdjan Nesic

Institute for Corrosion and Multiphase Flow Technology, Department of Chemical and Biomedical Engineering, Ohio University, Athens, OH 45701, USA

ARTICLE INFO

Article history:
Received 20 September 2018
Received in revised form
3 December 2018
Accepted 4 December 2018
Available online 4 December 2018

Keywords:
Corrosion
Mild steel
Hydrogen sulfide
Mechanism
Cathodic

ABSTRACT

In the context of H_2S corrosion of mild steel, the direct electrochemical reduction of H_2S is currently believed to be the main contribution of this species to cathodic currents. That is perhaps due to the distinct behavior of the cathodic polarization curves observed in the presence of H_2S, as compared to those obtained in strong acids solutions or in the presence of other weak acids such as carboxylic acids and carbonic acid. In the presence of aqueous H_2S, the cathodic polarization curves show a "double wave" shape, that is widely considered to be the result of the direct reduction of H_2S. In the present study, the mechanism of H_2S corrosion of mild steel is theoretically investigated with the focus on the buffering ability of H_2S. It is shown that all characteristic behaviors of cathodic currents that were previously associated with the direct reduction of H_2S, including the "double wave", can be fully explained in terms of the H_2S dissociation reaction and its buffering effect. In order to further evaluate this mechanistic argument, a comprehensive mathematical model for the H_2S system was developed and the calculated cathodic polarization curves were compared with the existing experimental data in the open literature. The results showed that the model, built with H^+ reduction as the sole cathodic reaction, is able to reasonably capture all characteristic behavior of cathodic currents, further supporting this mechanistic argument.

1. Introduction

In the presence of an aqueous medium, the hydrogen sulfide (H_2S) in the gas phase can dissolve and dissociate according to equilibrium Reactions (1) to (3). As a weak acid, H_2S is only partially dissociated in the aqueous phase, forming a chemical equilibria system. The presence of these sulfide species in the solution is believed to dramatically influence the corrosion process, both due to their electrochemical tendencies and perhaps more importantly, due to their contribution in formation of a corrosion product layer, and localized corrosion [1–5].

$$H_2S_{(g)} \rightleftharpoons H_2S_{(aq)} \quad (1)$$

$$H_2S_{(aq)} \rightleftharpoons HS^-_{(aq)} + H^+_{(aq)} \quad (2)$$

$$HS^-_{(aq)} \rightleftharpoons S^{2-}_{(aq)} + H^+_{(aq)} \quad (3)$$

The present study is focused on the mechanism of H_2S contribution to the cathodic currents in the context of mild steel corrosion. The acidic corrosion of steel in the presence of H_2S is believed to be the result of electrochemical dissolution of iron (oxidation partial of Reaction (4)) as the main anodic reaction, accompanied by a series of cathodic hydrogen evolving reactions, shown as the reduction partials of Reactions (5)–(7). These include the hydrogen ion (H^+) and water (H_2O) reduction (Reactions (5) and (7), respectively), which are well-known processes in metallic corrosion in acidic aqueous systems. Furthermore, the hydrogen-evolving reaction due to the direct reduction of H_2S (Reaction (6)) is presumed to be significantly contributing to the cathodic currents [6–15]. The relative significance of these cathodic reactions is thought to be defined mainly by the solution pH and H_2S partial pressure that specify the concentration of the involved electroactive species.

$$Fe^{2+} + 2e^- \rightleftharpoons Fe \quad (4)$$

* Corresponding author.
E-mail address: ak702711@ohio.edu (A. Kahyarian).

https://doi.org/10.1016/j.electacta.2018.12.029
0013-4686/

$$H^{+}_{(aq)} + e^{-} \rightleftharpoons 1/2 H_{2\,(g)} \quad (5)$$

$$H_2S_{(aq)} + e^{-} \rightleftharpoons 1/2 H_{2\,(g)} + HS^{-}_{\ (aq)} \quad (6)$$

$$H_2O_{(aq)} + e^{-} \rightleftharpoons 1/2 H_{2\,(g)} + OH^{-}_{\ (aq)} \quad (7)$$

The arguments related to the electrochemical contribution of H_2S to cathodic currents can be found in studies as early as 1965 as reported by Bolmer [6]. The direct H_2S reduction reaction was also believed to contribute to the observed cathodic currents obtained in rotating disk experiments by Morris et al. [7]. In that study, the authors noted that in the presence of H_2S, the H^+ reduction limiting current is significantly increased, while the behavior of the charge transfer controlled range of currents remained un-affected. That behavior was attributed to the direct reduction of H_2S, while no solid experimental proof was put forward. Following this trend in the subsequent studies, the direct reduction of H_2S was considered as the governing mechanism of corrosion in H_2S system [8–12]. However, no systematic investigation of this mechanism was done until the more recent years. In 2013, Kittel et al. investigated the cathodic polarization curves of a H_2S containing solution on a stainless steel surface [13]. The previous reports on the significant effect of H_2S on the limiting current was confirmed by the authors in that study. Furthermore, the authors showed that in certain conditions a "double wave" shape appears in the polarization curves; an observation that was considered as further proof for the direct H_2S reduction reaction. The observed "double wave" was associated with the existence of two electrochemical reactions and their corresponding limiting currents, one being H^+ reduction and the other being direct H_2S reduction. The experimental findings of this study were further used to developed a mathematical model of the cathodic polarization behavior in H_2S containing solutions [14].

In another recent study [15], Zheng et al. investigated the mechanism of mild steel corrosion in the presence of H_2S (pH_2S up to 0.1 bar), across a wider range of experimental conditions. The effect of H_2S on the limiting current, and the existence of two limiting currents (i.e. the "double wave") was also reported in that study. The authors noted that both limiting currents, associated with the H^+ and H_2S reduction reactions, are the results of mass transfer limitation of the involved reactants. These observations led the authors to conclude that in H_2S containing solutions, the direct reduction of H_2S is a significant cathodic process. Zheng et al. [15] also developed an elementary mechanistic model [16] based on these findings, where a reasonable agreement with the experimental data was reported. The scope of this study was later extended to the case of corrosion under mixed CO_2/H_2S conditions [17].

In 2017, Esmaeely et al. reported a set of experimental polarization data at pH_2S of 1 bar on a mild steel surface [18]. The reported polarization curves were found to behave similarly to those obtained at lower H_2S partial pressures reported in the earlier studies [15,17]. The authors used a similar model to that proposed by Zheng et al. [15] to quantify their experimental data, where a reasonably good agreement between the modeled and measured polarization curves were reported. That led the authors to also conclude that the direct H_2S reduction reaction is significantly contributing to the cathodic currents in such systems [18].

When one broadens the perspective to the general topic of mild steel corrosion in the presence of weak acids (to also include CO_2 and carboxylic acid), it can be seen that in the last 15 years the mechanistic understandings of these processes have been evolving dramatically [19–25]. The main leap was made by the introduction of comprehensive mechanistic mathematical models [24,26–29] into corrosion studies, as reviewed elsewhere [16,30]. These models allowed the complex set of homogeneous chemical reactions, typical of the solutions containing CO_2, carboxylic acid, and also H_2S, to be coupled with mass transfer and surface electrochemical processes. The quantitative results obtained from these models were able to clearly demonstrate the effect of homogeneous chemical reactions on corrosion, particularly on cathodic currents [20,23,24,26,31]. Based on such analyses as well as carefully targeted experiments, it was demonstrated that the direct reduction of weak acids such as acetic acid and carbonic acid –previously considered an essential part of the corrosion mechanism– is in fact insignificant [19,21–23,32]. The contribution of these species is now known to be mainly the result of their natural buffering ability as weak acids [19,21–23,32]. In typical environmental conditions seen in corroding systems, weak acids such as acetic acid and carbonic acid readily dissociate and buffer the surface pH, leading to a significant increase in the observed limiting current. That results in increased corrosion rates when it is controlled by the cathodic limiting current.

However, in mechanistic discussions of H_2S corrosion the buffering effect of this species has remained a largely neglected aspect. This may be partially due to the seemingly large pKa of H_2S and simplistic quantification of the results based on elementary mechanistic models, such as that developed by Zheng et al. [15,17]. These types of models are not able to properly represent the complex solution chemistry at the vicinity of the metal surface, as discussed in details elsewhere [16,30]. Considering the recent developments in mechanistic understanding of the abovementioned corrosion scenarios, one may expect H_2S (as a weak acid) to also exhibit a significant buffering ability, at least in a certain range of environmental conditions.

In the present study, the effect of homogeneous dissociation of H_2S inside the diffusion boundary layer on the polarization response of the system was investigated theoretically. For that purpose, a comprehensive mathematical model was developed that fully incorporates the effect of homogeneous reactions and transport processes on surface concentration of H^+. As discussed further below, the results showed that the buffering effect of H_2S is indeed significant in nearly all typically conditions encountered in the oil and gas production and transmission industry. The increased limiting currents and the observed "double wave" were readily explained by the homogeneous H_2S dissociation reaction, with no need to assume H_2S as an electrochemically active species. In order to further validate these observations, the existing experimental data reported in some recent studies [15,18] were compared with those obtained from this model.

2. Mathematical model

2.1. Water chemistry

Water chemistry calculation is the first step in a quantitative analysis of any corroding system, which is essential in obtaining the concentrations of the involved chemical species. Upon dissolution in water, the dissolved H_2S, as a diprotic weak acid, is partially dissociated to form HS^- and H^+. The HS^- itself can further dissociate to from another H^+ and S^{2-}. This reaction sequence is described by chemical Reactions (1) to (3). In an aqueous solution, the dissociation of water also occurs as shown by Reaction (8).

$$H_2O_{(l)} \rightleftharpoons OH^{-}_{(aq)} + H^{+}_{\ (aq)} \quad (8)$$

The dissolution of H_2S in water (equilibrium Reaction (1)) can be described according to Henry's law, assuming ideal conditions:

$$\frac{C_{H_2S_{(aq)}}}{p_{H_2S_{(g)}}} = H_{H_2S} \tag{9}$$

where $C_{H_2S_{(aq)}}$ (M) is the concentration of the dissolved H_2S, $p_{H_2S_{(g)}}$ is the partial pressure of H_2S (bar), and H_{H_2S} is the Henry's constant, as shown in Table 1.

The chemical equilibria of the dissociation Reactions (2) and (3) can be expressed mathematically via Equations (10) and (11), with K_{H_2S} and K_{HS^-} being their corresponding equilibrium constants as shown in Table 1.

$$\frac{C_{HS^-_{(aq)}} C_{H^+_{(aq)}}}{C_{H_2S_{(aq)}}} = K_{H_2S} \tag{10}$$

$$\frac{C_{S^{2-}_{(aq)}} C_{H^+_{(aq)}}}{C_{HS^-_{(aq)}}} = K_{HS^-} \tag{11}$$

The water dissociation reaction with the ionic product of K_w (see Table 1), can be expressed as:

$$C_{OH^-_{(aq)}} C_{H^+_{(aq)}} = K_w \tag{12}$$

At a given pH and pH_2S, the solution speciation can be obtained using the electro-neutrality constraint (Equation (13)) together with the equilibrium Equations (9)–(12). Fig. 1 demonstrates the results of such calculations for an open system at 0.1 and 1 bar H_2S partial pressures for a range of pH values.

$$\sum_i z_i C_i = 0 \tag{13}$$

2.2. Governing equations inside the diffusion boundary layer

Considering the heterogeneous nature of the electrochemical reactions, their rates are defined based on the local concentration of the active species at the metal surface, which are not known explicitly. However, the electrochemical response of a system can be obtained by solving the mass conservation law in the diffusion boundary layer. Such calculations allow the surface concentrations to be obtained based on the known bulk concentrations, when the appropriate relationships describing their concertation distribution inside the diffusion layer and at the electrode surface are used. The mass conservation law inside the diffusion boundary layer, is described as Equation (14), known as the Nernst-Planck Equation.

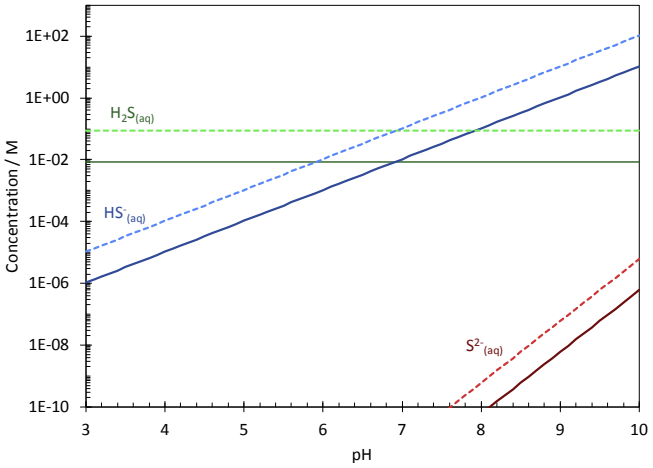

Fig. 1. The calculated solution speciation of H_2O/H_2S system at 30 °C, for 0.1 bar H_2S (solid lines), and 1 bar H_2S (dashed lines).

$$\frac{\partial C_i}{\partial t} = -\nabla \cdot N_i + R_i \tag{14}$$

Equation (14) describes the concentration distribution of species i, where N_i is the flux, and R_i is the source term that includes the consumption or production of species i by homogeneous chemical reactions. The flux of species i, is described as Equation (15) [33]:

$$N_i = -z_i u_i F C_i \nabla\phi - D_i \nabla C_i + \upsilon C_i \tag{15}$$

where the terms on the right-hand side describe the effect of electro-migration, molecular diffusion, and convective flow, respectively.

In the turbulent flow regime such as those observed in transmission pipelines or in laboratory conditions (e.g. rotating cylinder electrode test apparatus), the velocity term in Equation (15) cannot be specified without elaborate calculations. Hence the effect of turbulent flow in such scenarios is expressed by the aid of turbulent diffusion concept, with D_t representing the eddy diffusivity [34]. Hence Equation (15) is restated as Equation (16) for turbulent flow:

$$N_i = -z_i u_i F C_i \nabla\phi - (D_i + D_t)\nabla C_i \tag{16}$$

In typical pipe flow, rotating cylinder, rotating disc, etc., flow

Table 1
Equilibrium and kinetic rate constants of the H_2O/H_2S system.

Parameter	Reference
[a] $K_w = (10^{-3}\rho_w)^2\ 10^{\left(a1+\frac{a2}{T}+\frac{a3}{T^2}+\frac{a4}{T^3}+\left(a5+\frac{a6}{T}+\frac{a7}{T^2}\right)\log(10^{-3}\rho_w)\right)}$	[47]
(M^2) $a_1 = -4.098$, $a_2 = -3245.2$, $a_3 = 2.2362E5$, $a_4 = -3.984E7$, $a_5 = 13.957$, $a_6 = -1262.3$, $a_7 = 8.5641E5$	
$H_{H_2S} = (10^{-3}\rho_w)\ 10^{-\left(b_1+b_2\ T+b_3\ T^2+\frac{b_4}{T}+b_5\ \log(T)\right)}$	[48]
($M.bar^{-1}$) $b_1 = 6.343E2$, $b_2 = 2.709$ E−1, $b_3 = -1.113E-4$, $b_4 = -1.6719E4$, $b_5 = -2.619E2$	
$K_{H_2S} = (10^{-3}\rho_w)\ 10^{\left(c_1+c_2\ T+c_3\ T^2+\frac{c_4}{T}+c_5\ \ln(T)\right)}$	[49]
(M) $c_1 = 7.8243945E2$, $c_2 = 3.61261E-1$, $c_3 = -1.6722E-4$, $c_4 = -\ 2.05657315E4$, $c_5 = -\ 1.42741722E2$	
$K_{HS^-} = 10^{-17.4}$ (M)	[43]
$k_{b,H_2S} = 7.5 \times 10^{11}$ ($M^{-1}.s^{-1}$)	Estimated
$k_{b,HS^-} = 1 \times 10^{11}$ ($M^{-1}.s^{-1}$)	Estimated
$k_{b,w} = 1.4 \times 10^{11}$ ($M^{-1}.s^{-1}$)	[50,51]

[a] ρ_w is the density of water in kg.m-3 as shown in Table 3.

Table 2
Reference diffusion coefficients at 25 °C.

Species	Diffusion coefficient × 10^9/(m^2/s)	Reference
H_2S	1.93	[52]
HS^-	1.731	[53]
S^{2-}	1.5	Estimated
H^+	9.312	[33]
OH^-	5.273	[53]
Na^+	1.334	[33]
Cl^-	2.032	[33,53]

geometries, only the flux component perpendicular to the metal surface (here denoted by x) are relevant (in Equations (15) and (16)). Also, the mobility of ions can be defined by the Nernst-Einstein relationship ($u_i = D_i/RT$), with the diffusion coefficients listed in Table 2. Hence, the equations above can be simplified to Equations (17) and (18):

$$N_i = -(D_i + D_t)\frac{\partial C_i}{\partial x} - \frac{z_i D_i F C_i}{RT}\frac{\partial \phi}{\partial x} \tag{17}$$

$$\frac{\partial C_i}{\partial t} = \frac{\partial}{\partial x}\left((D_i + D_t)\frac{\partial C_i}{\partial x}\right) + \frac{z_i D_i F}{RT}\frac{\partial}{\partial x}\left(C_i\frac{\partial \phi}{\partial x}\right) + R_i \tag{18}$$

The eddy diffusivity distribution throughout the boundary layer of a fully developed turbulent flow can be obtained from the empirical equation suggested by Arvanith [35]:

$$D_t = \nu\,\frac{0.0007\,x^{+3}}{\left[1 + 0.00405x^{+2}\right]^{1/2}} \tag{19}$$

where ν is the kinematic viscosity ($m^2.s^{-1}$), and x^+ is the dimensionless distance from the wall defined as following, with x being the distance from the wall (m), τ_w being the wall shear stress (pa), and ρ being the fluid density ($kg.m^{-3}$).

$$x^+ = \frac{x\left(\tau_w/\rho\right)^{1/2}}{\nu} \tag{20}$$

Equation (19) is valid for x^+<30 and it is universal for all turbulent flow when appropriate dimensionless parameters are used. The relationships for the physical properties of water used in this study are listed in Table 3.

The wall shear stress, τ_w, in Equation (20), is a function of Fanning friction factor (C_f) as shown by Equation (21), which is a function of the Reynolds number (Re). The Reynolds number carries the turbulence and the geometry specific information in this set of equations.

$$\tau_w = 1/2\,\rho C_f V^2 \tag{21}$$

In Equation (21), V is the average flow velocity ($m.s^{-1}$), and ρ is the fluid density ($kg.m^{-3}$). The friction factor in a turbulent flow regime is obtained by the correlation of Swamee and Jain [36] for Darcy friction factor ($C_d = 4C_f$) (Equation (22)), which is essentially an explicit derivation of the well-known Colebrook-White correlation [37]. Noting that the first term inside the logarithm in Equation (22), accounts for the effect of surface roughness (ε) on the friction factor (here assumed to be zero).

$$C_d = 0.25\left[\log\left(\frac{\varepsilon/D_{eq}}{3.7} + \frac{5.74}{Re^{0.9}}\right)\right]^{-2} \tag{22}$$

As mentioned above, the rate of consumption or production of the chemical species by homogeneous chemical reactions are incorporated in these calculations through the R_i term in Equation (18). The rate of chemical reaction j involving species i, represented in general form as Reaction (23), is expressed as Equation (24).

$$\sum_{r=1}^{n_r} C_r \rightleftharpoons \sum_{p=1}^{n_p} C_p \tag{23}$$

$$R_j = k_{f,j}\prod_{r=1}^{n_r} C_r - k_{b,j}\prod_{p=1}^{n_p} C_p \tag{24}$$

where k_{fj} and k_{bj} are the reaction rate constants of the forward and backward reactions. The relevant chemical reactions, in the current system are: the dissociation of H_2S, HS^-, and H_2O. The kinetic rate constants for these reactions used in the present model can be found in Table 1. For each chemical species, R_i is the sum of the rates of all j chemical reactions involving this species, as shown in Equation (25). Here, the rate of reaction is expressed as a positive value when species i is produced, and as a negative value when it is consumed, and $s_{i,j}$ is the stoichiometric coefficient of species i in reaction j.

$$R_i = \sum_j R_j\, s_{i,j} \tag{25}$$

In addition to the concentration of species, the potential of the solution inside the diffusion boundary layer must be specified in order to calculate the effect of electro-migration, as seen in Equation (18). This parameter can be obtained by including the electroneutrality constraint in calculations, as shown by Equation (13).

2.3. Initial and boundary conditions

As a second order partial differential equation, Equation (18) can only be solved if the appropriate boundary and initial conditions are specified. The initial condition (for $t = 0$) was specified as constant known concentrations of chemical species defined by the chemical equilibria obtained from water chemistry calculations.

At the bulk solution boundary, where $x = \delta$, concentrations of chemical species remain unchanged at all times (for $t \geq 0$). The boundary conditions at the metal/solution interface are specified in term of the known flux of the chemical species, defined by

Table 3
Temperature dependence of physiochemical parameters.

Parameter	Relationship	Reference
Water density/(kg/m^3)	$\rho_w = 753.596 + 1.87748\,T - 0.003562\,T^2$	[24]
Water viscosity/(cP)	$\mu = \mu_{ref}10^{\left(\frac{1.1709\,(T_{ref}-T) - 0.001827(T_{ref}-T)^2}{(T-273.15)+89.93}\right)}$ $T_{ref} = 293.15\,K,\ \mu_{ref} = 1.002\,cP$	[54]
Diffusion coefficient	$D_i = D_{i,ref}\frac{T}{T_{ref}}\frac{\mu_{ref}}{\mu}$	[33]

Table 4
Summary of equations used in the mathematical model.

Electrode surface boundary	
$N_i\|_{x=0} = -\frac{s_{ij} i_j}{n_j F}$	For electro-active species
$N_i\|_{x=0} = 0$	For non-active species
$\sum_i z_i C_i = 0$	
Diffusion boundary layer	
$\frac{\partial C_i}{\partial t} = \frac{\partial}{\partial x}\left((D_i + D_t)\frac{\partial C_i}{\partial x}\right) + \frac{z_i D_i F}{RT}\frac{\partial}{\partial x}\left(C_i \frac{\partial \phi}{\partial x}\right) + R_i$	For all species
$\sum_i z_i C_i = 0$	
Bulk boundary conditions	
$C_i = C_i^b$	
$\Phi = 0$	Arbitrary reference potential

electrochemical reactions. For an electroactive chemical species, the flux at the metal (electrode) surface is equal to the rate of its consumption or production by the electrochemical reactions. For species *i*, involved in an electrochemical reaction:

$$N_i|_{x=0} = -\frac{s_i i}{nF} \tag{26}$$

where the negative sign in Equation (26) account for the sign conventions imbedded in flux, current density and stoichiometric coefficient (s_{ij}) terms.

The present study is focused on the cathodic currents, therefore, the anodic iron dissolution is not included in the present analysis. Since water reduction reactions is only significant at much lower potentials than those where reduction of H^+ ion is relevant, it was omitted as well. Furthermore, the present study is testing the hypothesis whether the polarization curves can be explained without considering the direct reduction of hydrogen sulfide (Reaction (6)), hence, the only electrochemical reaction considered in the present model is the one describing the H^+ reduction.

The cathodic current density resulting from H^+ reduction was calculated in the form shown by Equation (27). The kinetic parameters, including transfer coefficient $\alpha_{H^+} = 0.5$, the reaction order $m_{H^+} = 0.5$, and the reaction rate constant $k_{0H^+} = 1.2E-8\ mol^{0.5} m^{-0.5} s^{-1}$ used in this model, were estimated based on the experimental data previously reported in the literature as discussed in the following section.

$$i_{c,H^+} = -n_{H^+} F k_{0H^+} C_{H^+}^{s\ m_{H^+}} e^{\left(\frac{-\alpha_{H^+} n_{H^+} F\left(E_{app} - E_{0H^+}\right)}{RT}\right)} \tag{27}$$

The flux of non-electroactive species at the metal surface is zero:

$$N_i|_{x=0} = 0 \tag{28}$$

The flux Equations (27) and (28) describe the metal surface boundary conditions for all chemical species. Considering that N_i appears in these relationships, the solution potential should also be specified at the solution/metal boundary. This can be done similar to that in the governing equations by invoking the electroneutrality constraint as described by Equation (13), and the known fluxes of species.

2.4. Numerical solution

The mathematical relationships used to develop a comprehensive mathematical model are summarized in Table 4. These equations form a set of non-linear, coupled, partial differential equations. Considering the one-dimensional spatial domain, the solution can be obtained using a simple finite difference method. This is a common numerical technique used for solving differential equations, including those describing electrochemical systems [16,21,33].

The partial differential equations are discretized using second order Taylor's series approximations. The spatial derivative approximations for non-uniform spatial grid used in this study are shown in Table 5 for a function $f(x)$, where $\Delta x_j = x_j - x_{j-1}$ is the distance between the two adjacent nodes. In the present model the grid size is allowed to grow linearly with an expansion factor of 1.1 from the initial value of $\Delta x = 50$ nm adjacent to the metal surface.

The time integration is done explicitly, using Euler approximation. The resulting algebraic equations can be written in a matrix format, as a tri-diagonal coefficient matrix multiplied by a vector of the unknown concentrations and solution potential. The solution for each time step can then be obtained by inverting this matrix. The algorithm used here was Neman's "BAND" open-source code, where the solution is obtained by using the LU decomposition method [33]. The presence of nonlinear terms, such as those arising from the electro-migration or chemical reaction terms, means that some of the elements in the coefficient matrix are a function of other concentrations and/or potential, which are not explicitly known. In this approach, the solution of the equations was obtained iteratively by using an initial guess for the unknown terms of the coefficient matrix —usually the last calculated value— until the desired accuracy ($R^2 = 10^{-12}$) was achieved. The time step was then advanced and the whole process was repeated.

3. Results and discussion

3.1. A theoretical discussion

Let us first entertain the idea that the buffering effect of H_2S can become significant if the environmental conditions are favorable. This is an expected behavior of any weak acid as a result of its partial dissociation in an aqueous environment. As shown in the water chemistry calculations, the extent of dissociation is pH dependent. Considering the recent findings in similar systems, weak acids with relatively low pKa (about 4) such as acetic acid and

Table 5
Derivative approximation for a non-uniform grid.

First order derivative, central approximation		
$f'(x_i) = a_i f(x_{i-1}) + b_i f(x_i) + c_i f(x_{i+1})$		
$a_i = -\frac{\Delta x_{i+1}}{\Delta x_i(\Delta x_i + \Delta x_{i+1})}$	$b_i = \frac{\Delta x_{i+1} - \Delta x_i}{\Delta x_i \Delta x_{i+1}}$	$c_i = \frac{\Delta x_i}{\Delta x_{i+1}(\Delta x_i + \Delta x_{i+1})}$
First order derivative, three point forward approximation		
$f'(x_i) = a_i f(x_i) + b_i f(x_{i+1}) + c_i f(x_{i+2})$		
$a_i = -\frac{2\Delta x_{i+1} + \Delta x_{i+2}}{\Delta x_{i+1}(\Delta x_{i+1} + \Delta x_{i+2})}$	$b_i = \frac{\Delta x_{i+1} + \Delta x_{i+2}}{\Delta x_{i+1} \Delta x_{i+2}}$	$c_i = -\frac{\Delta x_{i+1}}{\Delta x_{i+2}(\Delta x_{i+1} + \Delta x_{i+2})}$
Second order derivative, central approximation		
$f''(x_i) = a_i f(x_{i-1}) + b_i f(x_i) + c_i f(x_{i+1})$		
$a_i = \frac{2}{\Delta x_i(\Delta x_i + \Delta x_{i+1})}$	$b_i = -\frac{2}{\Delta x_i \Delta x_{i+1}}$	$c_i = \frac{2}{\Delta x_{i+1}(\Delta x_i + \Delta x_{i+1})}$

carbonic acid are strong buffers [21–23]. This means that their equilibrium and kinetic properties allow them to readily dissociate as the pH is increased, for example at the metals surface under mass transfer limitation. In terms of reaction kinetics, the association of H_2S is categorized as "diffusion controlled", similar to association of water, carbonic acid, and acetic acid [38]. The term "diffusion controlled" refers to reactions with extremely high rates that occur as soon as the reactants "collide" [38–40]. With pKa of about 7, H_2S appears to be thermodynamically and kinetically capable to exhibit, at least to some extent, similar buffering ability as that observed for carbonic acid and carboxylic acids [19,21,41,42].

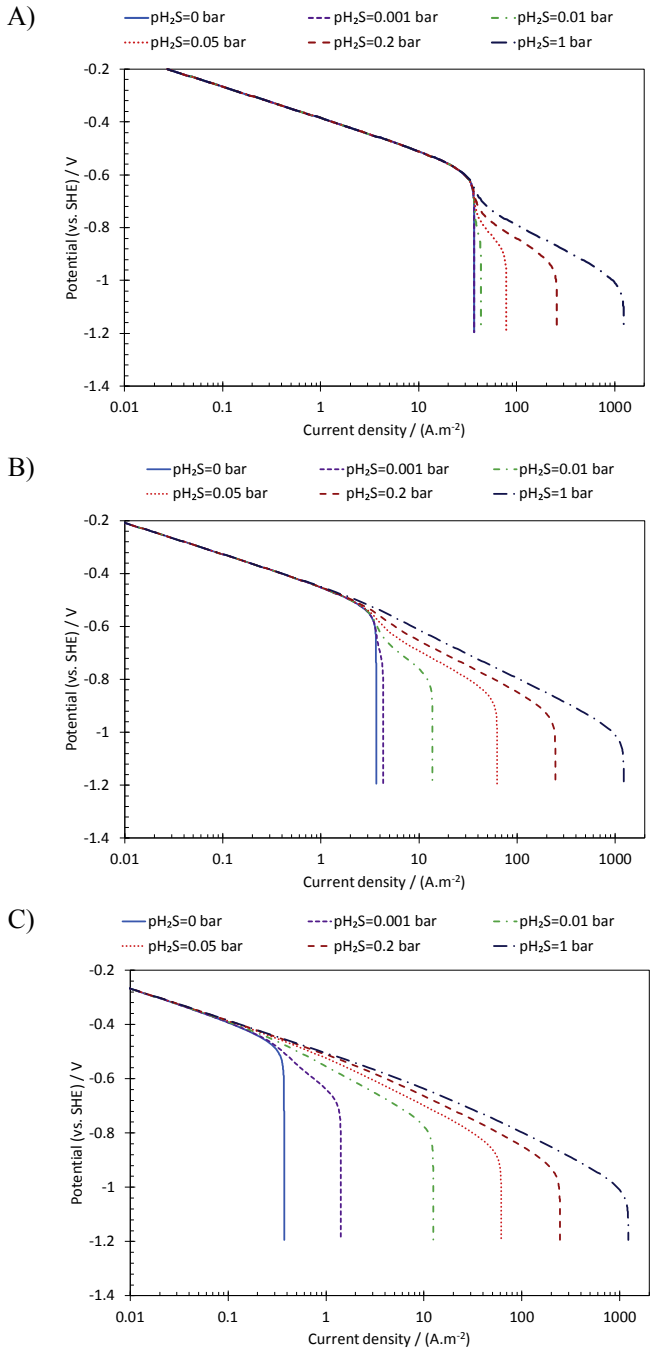

Fig. 2. Simulated steady state cathodic polarization behavior of acidic solutions containing H_2S, at 25 °C, 0.1 M NaCl, 2 m s^{-1} flow in a pipe with 0.012 m ID. A) pH 3. B) pH 4. C) pH 5.

The significance of the buffering ability of H_2S can be discussed theoretically in terms of simulated cathodic polarization curves, generated by the mathematical model described above. In this model, it was assumed that H^+ reduction is the only cathodic reaction (no direct reduction of H_2S). Fig. 2, demonstrates the predicted steady state polarization curves for the pH range from 3 to 5 and pH_2S of 0–1 bar. The results show that the buffering effect of H_2S is indeed significant at almost all conditions, which leads to a significant increase in the observed cathodic currents with increasing pH_2S. Furthermore, the characteristic cathodic "double wave" was also seen in the predicted voltammograms, even though it was previously associated with an additional electrochemical reaction – direct reduction of H_2S [13–15,17,18].

As it is clearly seen, the first limiting current can be associated with the mass transfer limitation related to H^+ reduction, which is not affected by pH_2S, and remains constant at a constant pH. The second limiting current is due to the presence of H_2S in the solution. As the pH is increased, the potential at which this wave is observed shifts towards more positive potentials. Also, the pH_2S at which the second wave appears decreases with increasing pH. On the other hand, the characteristic double wave shape rapidly diminishes at higher pH values. Considering that the predicted results are solely based on H^+ reduction, this behavior is a result of the relative dominance of two parallel processes that supply the H^+ to the electrode surface:

a) the mass transfer of H^+ from the bulk solution.
b) the dissociation of H_2S at the vicinity of the metal surface.

In order to further analyze the nature of the double wave, the calculated speciation at the metal surface during the polarization was analyzed. Fig. 3 illustrates the current response of the simulation at pH 3 and pH_2S of 0.2 bar on the secondary axis, versus the calculated surface pH on the horizontal axis. The behavior of the surface concentration of H_2S and HS^- are shown on the primary vertical axis of the same graph. As it is seen in Fig. 3, up to the current density of about 10 A.m^{-2}, the surface pH remains practically unchanged. That corresponds to the charge transfer controlled cathodic current range observed in Fig. 2A. In this range, the surface concentration of all species is the same as that in the bulk solution. As the first limiting current density is reached at about 40 A.m^{-2}, surface pH starts to increase, as expected in a mass transfer limiting

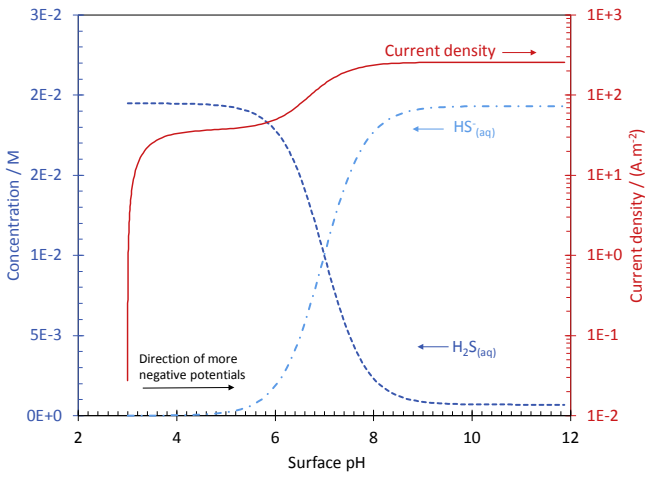

Fig. 3. The relationship between the calculated surface pH and the surface concentration of H_2S and HS^-, on the primary vertical axis, and the calculated current density, on the secondary vertical axis. Conditions: 25 °C, 2 m s^{-1} in a pipe with 0.012 m ID, pH 3, $pH_2S = 0.2$ bar, and the potential range from −0.2 to −1.2 V vs. SHE.

scenario. Even though the current density does not increase in this range, the surface pH increases as the potential (the driving force of the reaction) is shifted to more negative values. Ultimately, at some negative potential, the surface pH reaches a sufficiently high value where the dissociation of H_2S is favored, leading to a significant generating of H^+ at the surface. This process results in a notable influence on polarization curves at surface pH of about 5 and reaches its maximum at about 9. The pH where H_2S and HS^- concentration trends cross occurs near the pKa value of H_2S. Considering the higher pKa of HS^- (about 17) [43], no significant contribution from this reaction is expected in the present conditions.

Based on the discussion above, the reason why the double wave shape is not always observed should be sought in the behavior of the surface pH and the extent of H_2S dissociation. That is, the increased surface pH when the mass transfer limited current of H^+ reduction is reached. Take for example the case of a bulk pH of 5, this suggests the surface pH rapidly reaches the pH 6–7 (1–2 units higher than the bulk pH) when the limiting current is reached, which is within the range that favors H_2S dissociation. That means at bulk pH of 5 the conditions are such that H_2S readily dissociates when the limiting current is approached and hence, a double wave is not clearly observed as shown in Fig. 2C. On the other hand, at bulk pH of 3, the surface pH favorable for H_2S dissociation is only reached at potentials substantially into the H^+ reduction limiting current range (see Fig. 3); thus, the double wave is observed in an extended pH_2S range of Fig. 2A.

3.2. Experimental verification

In order to further examine the validity of the theoretical argument above, the results obtained from the model prediction were compared with the experimental data reported in the literature. The experimental data were taken from two recent studies by Zheng et al. [15] and Esmaeely [18] et al., who reported a systematic investigation of the electrochemical behavior of H_2S corrosion of mild steel over a wide range of experimental conditions (pH 3 to pH 5 and pH_2S from 0 to 1 bar).

The experiments in these studies were done using rotating cylinder electrodes (RCE) while the model is created for a straight pipe flow geometry. In order to properly estimate the equivalent mass transfer conditions [44], the mass transfer coefficient for RCE from the Eisenberg [45] equation was equated with the one obtained from a relationship proposed by Berger and Hau [46] for straight pipe flow. The equivalent flow velocity (v_{pipe} in $m.s^{-1}$) is then (29):

$$v_{pipe} = 0.5610\, Sc^{0.03}\, \nu^{0.186} \Omega_{RCE}^{0.814} \frac{d_{RCE}^{1.628}}{d_{pipe}} \quad (29)$$

where Ω_{RCE} is the angular velocity of the RCE electrode ($rad.s^{-1}$), and other parameters have their common electrochemical meaning.

The comparison of the predicted cathodic currents, solely based on H^+ reduction (including the buffering effect of H_2S), and experimental data are shown in Figs. 4 and 5. A good agreement with the experimental data was found, where the model was able to predict the main characteristic features of the cathodic polarization curves. In previous studies by Zheng et al. [15] and Esmaeely [18] et al., the authors proposed a mechanistic model, where both H^+ and H_2S were considered to be reduced at the metal surface. Even though the present model does not include the direct reduction of H_2S, the simulated cathodic polarization curves were found to be at the same level of agreement with the experimental data, as those reported in the original studies [15,18].

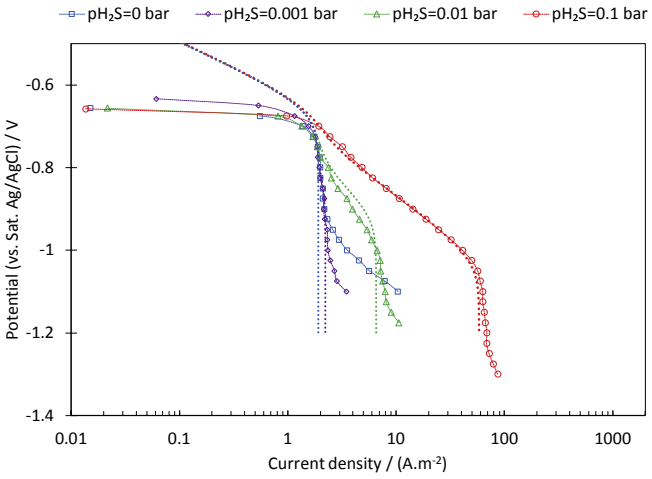

Fig. 4. Cathodic polarization curves at pH 4, 30 °C, 1000 rpm RCE (equivalent to 0.81 m s^{-1} pipe flow with 0.012 m ID), at various H_2S partial pressures. The points are measurements and the dotted lines show the results generated by the present model. The experimental data was taken from Zheng et al. [15].

In Fig. 4, showing data for pH 4 and H_2S partial pressures up to 0.1 bar, the limiting current densities were found to be in good agreement with the experimental data. The presence of the double wave, and its position was also reasonably predicted by the model. It is worthwhile to note that the current densities in the potential range between the two limiting currents show a clear dependence on the pH_2S. Nonetheless, they are properly estimated by the model solely based on H^+ reduction. This can be understood when considering the fact that this range of current densities is not controlled purely by the charge transfer process. At this range, the surface concentration of H^+ is defined by the H_2S dissociation reaction. Naturally, the increased concentration of H_2S results in an increased rate of dissociation and hence, higher concentration of H^+ at the surface. This process is of more significance in the results obtained at higher pH values as shown in Fig. 5.

Fig. 5 demonstrates the comparison of the model with the experimental data at 0.1 bar pH_2S as reported by Zheng et al. [15] and 1 bar as reported by Esmaeely et al. [18]. At elevated H_2S partial pressures, the reproducibility of the experiments were decreased as seen from the larger error bars. Even at such high H_2S partial pressure, the present model was found to agree reasonably well with the experimental polarization curves, where the main characteristic behaviors at all pH values were correctly predicted. That further validates the electrochemical mechanisms used in developing the model, suggesting the direct reduction of H_2S is not significant during cathodic polarization.

The results at pH 5, as reported in Fig. 5C, are of particular significance for the generic argument about the characteristic shapes of cathodic polarization curves obtained in the presence of weak acids. At this particular condition, only one limiting current is observed following the downward sloping linear range. It can be deduced from Fig. 2C and above discussions, that the surface concentration of H^+ in this range of current densities is strongly influenced by the H_2S dissociation reaction and the current response of the system is not properly representing the kinetics of electrochemical processes. Nevertheless, based on its appearance, this linear range of current densities could be easily mischaracterized as a pure charge transfer controlled range with Tafel behavior, and erroneous conclusions could be reached about the reaction mechanism and rates [13–15,18]. This type of arguments was used by various authors, including Kittel et al. [13], Tribollet

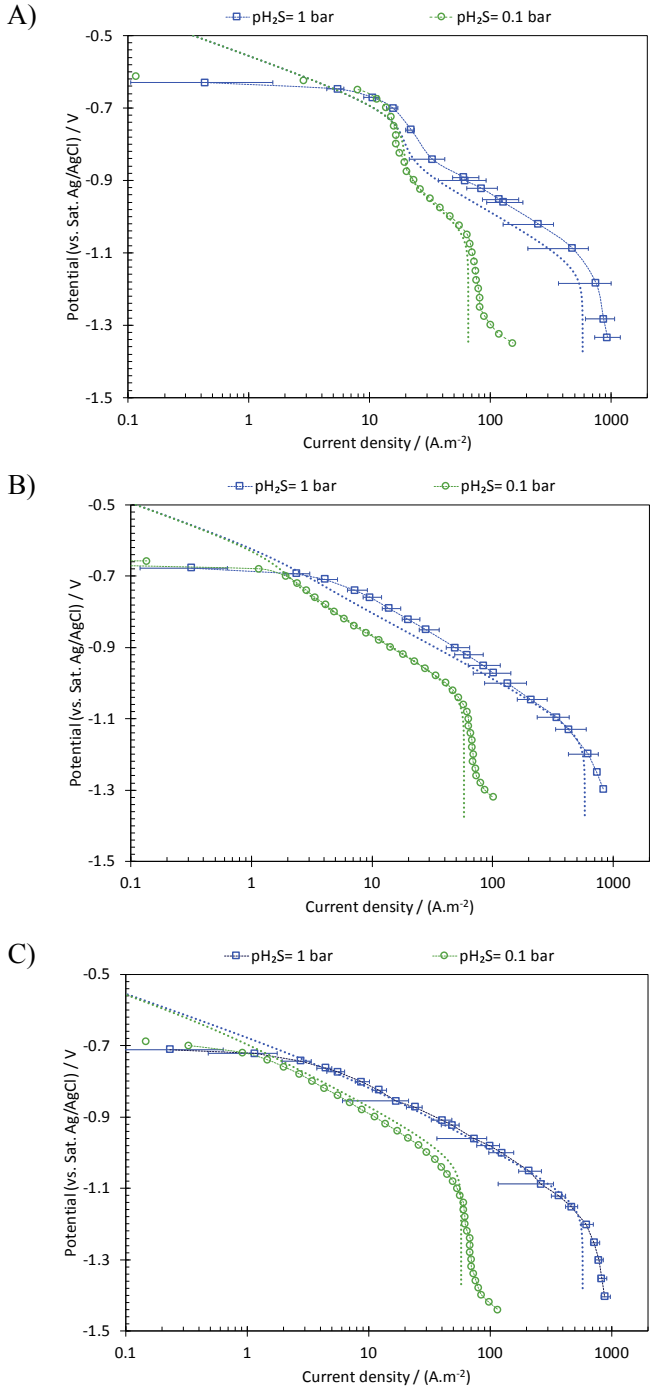

Fig. 5. Cathodic polarization curves at 30 °C, 1000 rpm RCE (equivalent to 0.81 m s^{-1} pipe flow with 0.012 m ID), at $pH_2S = 0.1$ bar (green circles) and $pH_2S = 1$ bar (blue squares) partial pressures and the dotted lines show the results from the present model. A) pH 3. B) pH 4. C) pH 5. The experimental data at $pH_2S = 0.1$ bar was taken from Zheng et al. [15], and the experimental data at $pH_2S = 1$ bar was taken from Esmaeely et al. [18].

et al. [14], Zheng et al. [15] and Esmaeely et al. [18] as evidence for the existence of direct reduction of H_2S and to determine its kinetic parameters. Indeed, unusually high Tafel slopes and difficult to explain reaction orders were derived this way for the direct H_2S reduction reaction [13–15,18]. For example, the experimental cathodic currents shown in Fig. 5C, if associated with the direct reduction of H_2S, show Tafel slopes of 200 mV and 160 mV for 0.1 bar and 1 bar H_2S concentrations, respectively, and about 0.3 order dependence on H_2S concentration.

This discussion signifies the importance of using comprehensive quantitative calculations in analysis of the experimental data from such systems, similar to the approach used in this study. The simulated results as shown in Fig. 5, clearly demonstrate that such behavior is not related to direct reduction of H_2S. As argued above, the observed current densities in the range between the two limiting currents are not purely governed by the charge transfer kinetics, but rather they are affected by the kinetics of the H_2S dissociation, which defines the surface H^+ concertation. This range of current densities corresponds to the range of decaying surface H_2S concentrations, as seen in Fig. 3. The apparent H_2S dependence of the current densities is therefore the result of the increased rate of H_2S dissociation that leads to higher concentration of H^+ at the surface. The main difference between the present case of H_2S and that of acetic acid and carbonic acid is in the relatively lower pK_a and dissociation kinetics (~10^5 vs. ~10^8) for H_2S that results in observation of such behavior.

4. Conclusions

The theoretical analysis of polarization behavior of H_2S containing acidic solutions showed that the direct reduction of H_2S is insignificant at the conditions considered here. The increased limiting currents and the observed “double wave” behavior can be fully explained by the homogeneous dissociation of H_2S inside the diffusion boundary layer.

It is shown that the buffering effect of H_2S is observed when the surface pH approaches the pKa of this species. This behavior results in the observation of the secondary limiting current in lower bulk pH values and explains why the second wave is not observed as clearly in the solutions of higher bulk pH. The comparison of the results from the present model with experimental cathodic polarization curves showed that this mechanistic behavior remains valid for a wide range of conditions from pH 3 to 5 and H_2S partial pressures up to 1 bar.

Acknowledgements

The author would like to thank the following companies for their financial support: Anadarko, Baker Hughes, BP, Chevron, CNOOC, ConocoPhillips, DNV GL, ExxonMobil, M-I SWACO (Schlumberger), Multi-Chem (Halliburton), Occidental Oil Company, PTT, Saudi Aramco, SINOPEC (China Petroleum), and TOTAL.

References

[1] M.S. Wei Zhang, Bruce Brown, David Young, Srdjan Nesic, Factors Influencing Localized Corrosion of Mild Steel in Marginally Sour Environments, CORROSION, 2018. Paper No. 10548.
[2] M.A. Lucio-garcia, J.G. Gonzalez-rodriguez, M. Casales, L. Martinez, J.G. Chacon-nava, Effect of heat treatment on H_2S corrosion of a micro-alloyed C – Mn steel, Corros. Sci. 51 (2009) 2380–2386, https://doi.org/10.1016/j.corsci.2009.06.022.
[3] S. Gao, B. Brown, D. Young, M. Singer, Formation of iron oxide and iron sulfide at high temperature and their effects on corrosion, Corros. Sci. 165 (2018) 171–179, https://doi.org/10.1016/j.corsci.2018.02.045.
[4] S.N. Esmaeely, S. Nesic, Reduction reactions on iron sulfides in aqueous acidic solutions, J. Electrochem. Soc. 164 (2017) C664–C670, https://doi.org/10.1149/2.1381712jes.
[5] S.N. Esmaeely, G. Bota, B. Brown, S. Nešić, Influence of pyrrhotite on the corrosion of mild steel, Corrosion 74 (2018) 37–49, https://doi.org/10.5006/2505.
[6] P.W. Bolmer, Polarization of iron in H_2S-NaHS buffers, Corrosion 3 (1965) 69–75.
[7] D.R. Morris, The corrosion of steel by aqueous solutions of hydrogen sulfide, J. Electrochem. Soc. 127 (1980) 1228–1235, https://doi.org/10.1149/1.2129861.
[8] D.W. Shoesmith, The formation of ferrous monosulfide polymorphs during the corrosion of iron by aqueous hydrogen sulfide at 21°C, J. Electrochem. Soc. 127

(1980) 1007–1015, https://doi.org/10.1149/1.2129808.
[9] R. Galvan-Martinez, J. Mendoza-Flores, R. Duran-Romero, J. Genesca, Effect of turbulent flow on the anodic and cathodic kinetics of API X52 steel corrosion in H_2S containing solutions. A rotating cylinder electrode study, Mater. Corros. 58 (2007) 514–521, https://doi.org/10.1002/maco.200604038.
[10] R. Galvan-Martinez, J. Mendoza-Flores, R. Duran-Romero, J. Genesca-Llongueras, Effects of turbulent flow on the corrosion kinetics of X52 pipeline steel in aqueous solutions containing H_2S, Mater. Corros. 55 (2004) 586–593, https://doi.org/10.1002/maco.200303776.
[11] S. Arzola, J. Genescá, The effect of H_2S concentration on the corrosion behavior of API 5L X-70 steel, J. Solid State Electrochem. 9 (2005) 197–200, https://doi.org/10.1007/s10008-004-0579-9.
[12] S. Arzola, J. Mendoza-Flores, R. Duran-Romero, J. Genesca, Electrochemical behavior of API X70 steel in hydrogen sulfide-containing solutions, Corrosion 62 (2006) 433–443, https://doi.org/10.5006/1.3278280.
[13] J. Kittel, F. Ropital, F. Grosjean, E.M.M. Sutter, B. Tribollet, Corrosion mechanisms in aqueous solutions containing dissolved H_2S. Part 1: characterisation of H_2S reduction on a 316L rotating disc electrode, Corros. Sci. 66 (2013) 324–329, https://doi.org/10.1016/j.corsci.2012.09.036.
[14] B. Tribollet, J. Kittel, A. Meroufel, F. Ropital, F. Grosjean, E.M.M. Sutter, Corrosion mechanisms in aqueous solutions containing dissolved H_2S. Part 2: model of the cathodic reactions on a 316L stainless steel rotating disc electrode, Electrochim. Acta 124 (2014) 46–51, https://doi.org/10.1016/j.corsci.2012.09.036.
[15] Y. Zheng, B. Brown, S. Nešic, Electrochemical study and modeling of H_2S corrosion of mild steel, Corrosion 70 (2014) 351–365.
[16] A. Kahyarian, M. Singer, S. Nesic, Modeling of uniform CO_2 corrosion of mild steel in gas transportation systems: a review, J. Nat. Gas Sci. Eng. 29 (2016) 530–549, https://doi.org/10.1016/j.jngse.2015.12.052.
[17] Y. Zheng, J. Ning, B. Brown, S. Nesic, Electrochemical model of mild steel corrosion in a mixed H_2S/CO_2 aqueous environment, Corrosion 71 (2014) 316–325, 2014.
[18] S.N. Esmaeely, B. Brown, S. Nesic, Verification of an electrochemical model for aqueous corrosion of mild steel for H2S partial pressures up to 0.1 mpa, Corrosion 73 (2017) 144–154.
[19] A. Kahyarian, B. Brown, S. Nesic, Mechanism of cathodic reactions in acetic acid corrosion of iron and mild steel, Corrosion 72 (2016) 1539–1546, https://doi.org/10.5006/2177.
[20] A. Kahyarian, B. Brown, S. Nesic, Electrochemistry of CO_2 corrosion of mild steel: effect of CO_2 on iron dissolution reaction, Corros. Sci. 129 (2017) 146–151, https://doi.org/10.1016/j.corsci.2017.10.005.
[21] A. Kahyarian, A. Schumaker, B. Brown, S. Nesic, Acidic corrosion of mild steel in the presence of acetic acid: mechanism and prediction, Electrochim. Acta 258 (2017) 639–652, https://doi.org/10.1016/j.electacta.2017.11.109.
[22] T. Tran, B. Brown, S. Nešic, B. Tribollet, Investigation of the electrochemical mechanisms for acetic acid corrosion of mild steel, Corrosion 70 (2014) 223–229.
[23] E. Remita, B. Tribollet, E. Sutter, V. Vivier, F. Ropital, J. Kittel, Hydrogen evolution in aqueous solutions containing dissolved CO_2: quantitative contribution of the buffering effect, Corros. Sci. 50 (2008) 1433–1440, https://doi.org/10.1016/j.corsci.2007.12.007.
[24] M. Nordsveen, S. Nešić, R. Nyborg, A. Stangeland, A mechanistic model for carbon dioxide corrosion of mild steel in the presence of protective iron carbonate films - part 1: theory and verification, Corrosion 59 (2003) 443–456, https://doi.org/10.5006/1.3277592.
[25] S. Nešić, M. Nordsveen, R. Nyborg, A. Stangeland, A mechanistic model for carbon dioxide corrosion of mild steel in the presence of protective iron carbonate films—Part 2: a numerical experiment, Corrosion 59 (2003) 489–497, https://doi.org/10.5006/1.3277592.
[26] B.F.M. Pots, Mechanistic models for the prediction of CO_2 corrosion rates under multi-phase flow conditions, in: CORROSION, 1995. Paper No. 137.
[27] F.M. Song, D.W. Kirk, J.W. Graydon, D.E. Cormack, Predicting carbon dioxide corrosion of bare steel under an aqueous boundary layer, Corrosion 60 (2004) 736–748, https://doi.org/10.5006/1.3287866.
[28] F.M. Song, D.W. Kirk, J.W. Graydon, D.E. Cormack, CO_2 corrosion of bare steel under an aqueous boundary layer with oxygen, J. Electrochem. Soc. 149 (2002) B479–B486, https://doi.org/10.1149/1.1509068.
[29] F.M. Song, A comprehensive model for predicting CO_2 corrosion rate in oil and gas production and transportation systems, Electrochim. Acta 55 (2010) 689–700, https://doi.org/10.1016/j.electacta.2009.07.087.
[30] A. Kahyarian, M. Achour, S. Nesic, Mathematical modeling of uniform CO_2 corrosion, in: A.M. El-Sherik (Ed.), Trends Oil Gas Corros. Res. Technol., Elsevier, 2017, pp. 805–849.
[31] S. Nešić, M. Nordsveen, R. Nyborg, A. Stangeland, A mechanistic model for CO_2 corrosion with protective iron carbonate films, in: CORROSION, 2001. Paper No. 040.
[32] T. Tran, B. Brown, S. Nešić, Corrosion of mild steel in an aqueous CO_2 environment – basic electrochemical mechanisms revisited, in: CORROSION, 2015. Paper no. 671.
[33] J. Newman, K.E. Thomas-Alyea, Electrochemical Systems, third ed., Wiley-interscience, 2004.
[34] J.T. Davies, Chapter 3: eddy transfer near solid surfaces, in: Turbul. Phenom., Elserviere Inc., 1972, pp. 121–174.
[35] S. Aravinth, Prediction of heat and mass transfer for fully developed turbulent fluid flow through tubes, Int. J. Heat Mass Tran. 43 (2000) 1399–1408, https://doi.org/10.1016/S0017-9310(99)00218-5.
[36] P.K. Swamee, A.K. Jain, Explicit equations for pipe-flow problems, J. Hydraul. Div. 102 (1976) 657–664.
[37] C.F. Colebrook, C.M. White, Experiments with fluid friction in roughened pipes, Proc. R. Soc. A Math. Phys. Eng. Sci. 161 (1937) 367–381, https://doi.org/10.1098/rspa.1937.0150.
[38] M. Eigen, Proton transfer, acid-base catalysis, and enzymatic hydrolysis, Angew. Chem. Int. Ed. Engl. 3 (1964) 1–19.
[39] M. Eigen, L. De Maeyer, Self-dissociation and protonic charge transport in water and ice, Proc. R. Soc. London, Ser. A. 247 (1958) 505–533.
[40] M. Eigen, E. Eyring, Fast protolytic reactions in aqueous solutions of aminobenzoic acids, J. Am. Chem. Soc. 84 (1962) 3254–3256, https://doi.org/10.1021/ja00876a008.
[41] A. Kahyarian, B. Brown, S. Nesic, Mechanism of CO_2 Corrosion of Mild Steel: a New Narrative, CORROSION, 2018. Paper No. 11232.
[42] A. Kahyarian, B. Brown, S. Nesic, S. Ne, Technical note: electrochemistry of CO_2 corrosion of mild steel: effect of CO_2 on cathodic currents, Corrosion 74 (2018) 851–859, https://doi.org/10.5006/2792.
[43] A.A. Migdisov, A.E. Williams-Jones, L.Z. Lakshtanov, Y.V. Alekhin, Estimates of the second dissociation constant of H_2S from the surface sulfidation of crystalline sulfur, Geochem. Cosmochim. Acta 66 (2002) 1713–1725, https://doi.org/10.1016/S0016-7037(01)00896-1.
[44] D.C. Silverman, The rotating cylinder electrode for examining velocity-sensitive corrosion — A Review 60 (2004) 1003–1023.
[45] M. Eisenberg, C.W. Tobias, C.R. Wilke, Ionic mass transfer and concentration polarization at rotating electrodes, J. Electrochem. Soc. 101 (1954) 306–320, https://doi.org/10.1149/1.2781252.
[46] F.P. Berger, K.-F.F.-L. Hau, Mass transfer in turbulent pipe flow measured by the electrochemical method, Int. J. Heat Mass Tran. 20 (1977) 1185–1194, https://doi.org/10.1016/0017-9310(77)90127-2.
[47] W.L. Marshall, E.U. Franck, Ion product of water substance, 0-1000 °C, 1-10,000 bars New International Formulation and its background, J. Phys. Chem. Ref. Data 10 (1983) 295–304, https://doi.org/10.1063/1.555643.
[48] O.M. Suleimenov, R.E. Krupp, Solubility of hydrogen sulfide in pure water and in NaCl solutions, from 20 to 320 °C and at saturation pressures, Geochem. Cosmochim. Acta 58 (1994) 2433–2444, https://doi.org/10.1016/0016-7037(94)90022-1.
[49] O.M. Suleimenov, T.M. Seward, A spectrophotometric study of hydrogen sulphide ionisation in aqueous solutions to 350°C, Geochem. Cosmochim. Acta 61 (1997) 5187–5198, https://doi.org/10.1016/S0016-7037(97)00291-3.
[50] M. Eigen, Proton-transfer, acid-base catalysis, and enzymatic hydrolysis, Angew. Chem. Int. Ed. Engl. 3 (1964) 1–72.
[51] F.H. Stillinger, Proton transfer reactions and kinetics in water, Theor. Chem. Adv. 3 (1978) 177–234.
[52] A. Tamimi, E.B. Rinker, O.C. Sandall, Diffusion coefficients for hydrogen sulfide, carbon dioxide, and nitrous oxide in water over the temperature range 293–368 K, J. Chem. Eng. Data 39 (1994) 330–332, https://doi.org/10.1021/je00014a031.
[53] W.M. Haynes (Ed.), CRC Handbook of Chemistry and Physics, 84th ed., CRC Press LLC, 2004.
[54] L. Korson, W. Drost-Hansen, F.J. Millero, Viscosity of water at various temperatures, J. Phys. Chem. 73 (1969) 34–39, https://doi.org/10.1021/j100721a006.